Science Progress (2018), 101(4), 384–396
Paper 1800278 https://doi.org/10.3184/003685018X15360899653905

Current Commentary

Perovskites – some snapshots of recent developments

CHRISTOPHER J. RHODES

Fresh-lands Environmental Actions, 88 Star Road, Caversham, Berkshire RG4 5BE, UK
Email: cjrhodes@fresh-lands.com

Keywords: *perovskite, earth-abundant elements, stability, LED, laser, kesterite, solar cell, photovoltaic, PV, photocatalyst, pollutant degradation, phosphor, light converting layer, nanocrystal, quantum confinement, dynamics*

1. Introduction

The range of investigations into the use of 'perovskite' materials for light harvesting purposes[1–3] continues to broaden and advance seemingly inexorably, as is attested by the exponential growth in the number of publications that may be identified when this word is input into various databases, *e.g.* Scopus, as a search term[4], and which parallels both the remarkable increase in quantum efficiencies that have been attained[5], and the number of patents for perovskite photovoltaic devices granted since the year 2010[5]. In the main, the applications for perovskites, sought so far, concern solar energy production, due to their considerable promise as optoelectronic materials, and that they can be made cheaply using solution-based methods, and from earth-abundant elements. Although lead halide perovskites have been known[6] since 1893, it was not until 2009 that $CH_3NH_3PbI_3$ (Figure 1) was used as a sensitiser in solar cells, which gave a power-conversion efficiency of 3.8% (see ref. 7). One advantage of this material is that it has a direct bandgap of 1.55 eV, meaning that it absorbs visible light wavelengths from across the solar emission spectrum[8]. As a result of rapid progress in the development of new architectures and tailored compositions, in 2017, the power-conversion efficiency (PCE) had risen to 22.7% (see ref. 9), and in 2018, silicon-based tandem cells were reported with PCEs of up to 26.7% (see ref. 10) and 25.2% in 4-terminal and 2-terminal configurations, respectively[11]. The perovskite component is more efficient in utilising blue and green light, while light wavelengths in the red and infra-red region are more effectively harvested by silicon: hence, in combination, the two materials can absorb light further across the solar spectrum and generate more power than either can singly; on the basis of theoretical calculations, it is anticipated that an increase in the efficiency to 30% might soon be possible[11]. In regard to thin film perovskite solar cells, which it is thought should be possible to manufacture on a large scale and cheaply, an initial world record of 13.5%, as reported in 2017, has just been updated to 14.5% (see ref. 12). It is of further significance that larger arrays can be created by connecting together individual thin film cells with little loss in efficiency[12].

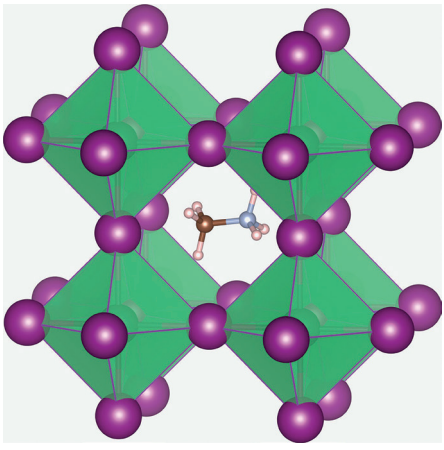

Figure 1 *$CH_3NH_3PbI_3$ structure. Methylammonium cation ($CH_3NH_3^+$) is surrounded by 12 nearest-neighbour iodide ions in corner-sharing PbI_6 octahedra. Credit: Christopher Eames* et al.*, https://upload.wikimedia.org/wikipedia/commons/d/df/CH3NH3PbI3_structure.png.*

According to the Shockley–Queisser formulation[13], in which all recombination events should ultimately be radiative, an efficient light-absorbing semiconductor should also be a good light-emitter, and indeed strong photoluminescence (PL) has been observed for perovskites, meaning that they might prove effective in light-emitting devices, as well as in solar cells[14]. In this regard, perovskite nanocrystals are potentially of particular importance, for which very high PL quantum efficiencies have been demonstrated, along with narrow emission linewidths (as is true of other kinds of quantum dot semiconductors), the ability to tune the colour of the emission across the entire range of the visible spectrum, and that they can be prepared by methods of colloidal synthesis. Specifically, typical 'full width at half maximum' linewidths are close to 0.1 eV (see ref. 8), the corresponding wavelength of which varies across the visible spectrum, and is around 35 nm, 12–15 nm, and 20 nm, in the red, blue-violet and green regions, respectively[8].The PL quantum yield may approach 100% for perovskite nanocrystals containing bromine[8], and is typically 60–70% for iodine[8], while chlorine-based analogues tend to exhibit lower values, of up to a maximum of around 10% (see ref. 8).

2. Fine-tuning the optical properties of perovkites

Due to the fact that it is possible to create perovskites containing mixtures of different halides, each with its own optical and band gap properties, the materials can be tuned so to emit wavelengths across the 400–700 nm range[15] (Figure 2). This may be achieved either by introducing an appropriate ratio of halide salts (*e.g.* PbI_2, $PbBr_2$, $PbCl_2$) in the colloidal synthesis, or by adding an excess of other halide ions (either Cl^- or I^-) to the solution of $CsPbBr_3$ nanocrystals, so that ion exchange occurs, with the complete or partial replacement of Br^- ions in the nanocrystals: when chlorine is incorporated in the nanocrystals, a blue shift of the PL wavelength occurs, or a red shift when iodine is included[15]. It is also possible to introduce other kinds of metal ions in place of lead, or to change the type of organic molecules present in the perovskite, with the effect of tuning the emission wavelengths into the near infrared or ultraviolet regions of the electromagnetic spectrum[15]. The band gap may also be 'widened' by varying the synthesis conditions such that the dimension of the

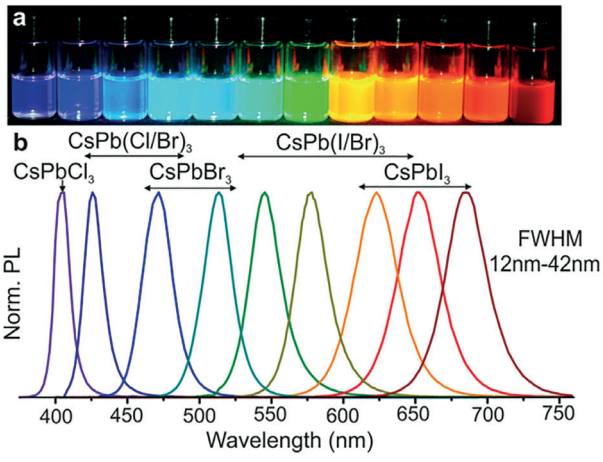

Figure 2 *Solutions of lead halide perovskite NCs of different halide composition under UV light illumination. (a) By changing the halogen (X) in the material, it is possible to obtain bright emitters across the red–violet spectral range, (b) corresponding PL profiles[17]. Reproduced with permission from ACS, https://pubs.acs.org/doi/abs/10.1021%2Fnl5048779. Further permissions related to the material excerpted should be directed to the ACS.*

nanocrystals can be brought down to the quantum confinement regime[15], and a blue shift of the PL wavelength occurs, as is exemplified in the following section.

3. Quantum confinement effect

Quantum confinement effects may become manifest when a dimension of a semiconductor is smaller than the Bohr radius of the exciton pair (M^+ ... e^-). This causes the energy levels to become quantised, as in individual molecules, rather than coalescing into the 'band structure' of bulk semiconductors[16]. (A quantum dot causes confinement in all three dimensions, a quantum wire in two dimensions, and a quantum well in just a single dimension. In an alternative terminology, which refers to the number of dimensions in which a confined particle can act as a free carrier, quantum dots, wires and wells are, respectively, termed as zero-, one- and two-dimensional potential wells.) Traditional (bulk) semiconductors lack versatility, since their band-gaps, and hence optical and electronic properties, cannot be easily changed, if at all; however, by tuning the size of the semiconductor particle, the band gap can be tailored for specific applications. The gap enlarges as the crystalline dimension decreases, so that the fluorescence wavelength shortens, and so the emitted light shifts toward the blue end of the visible spectrum. The calculated[15] exciton Bohr radius is 7 nm in all-inorganic $CsPbBr_3$ perovskite nanocrystals, and hence by changing the size of the crystals from 4 nm to 12 nm, the emission from these materials can be tuned from around 2.7 eV to 2.4 eV, which, as is shown in Figure 3, is in reasonable accord with a theoretical model[17]. The effect of quantum confinement is similarly apparent in organic–inorganic methylammonium lead halide perovskite nanocrystals[8,15], and overall can furnish a strategy for fine-tuning the emission wavelengths for semiconductors, with potential applications for various light-emitting devices.

4. LEDs for display applications

There are various potential advantages of using perovskites in LED applications, among which are a typically high colour purity of their electroluminescence

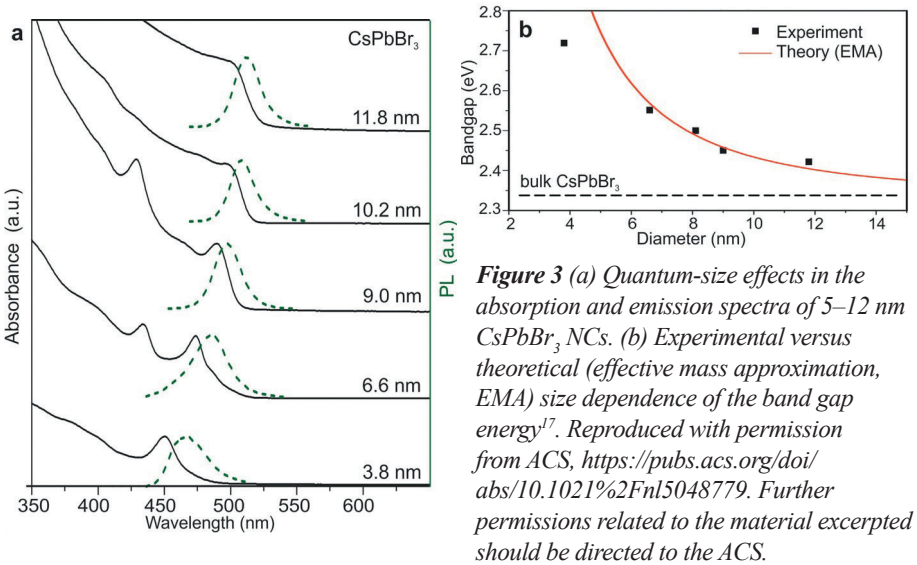

Figure 3 *(a) Quantum-size effects in the absorption and emission spectra of 5–12 nm $CsPbBr_3$ NCs. (b) Experimental versus theoretical (effective mass approximation, EMA) size dependence of the band gap energy[17]. Reproduced with permission from ACS, https://pubs.acs.org/doi/abs/10.1021%2Fnl5048779. Further permissions related to the material excerpted should be directed to the ACS.*

spectra, and a full width half maximum of ~ 15–25 nm, and (as already noted) that the emission wavelength (colour) can be tuned across the entirety of the visible solar spectrum[8,15]. Quantum dot perovskites have been demonstrated to give both a strong luminescence and a high external quantum yield, in part because the smaller grain size increases the possibility of radiative recombination by impeding the process of exciton diffusion. Indeed, encouragingly high LED performances have been obtained from amorphous perovskite quantum dots[15]. $CsPbX_3$ quantum dots have been explored, as an all-inorganic alternative for LED applications, in an attempt to circumvent the instability of hybrid organic–inorganic perovskites[8,15]. LEDs have also been made from perovskite nanoplatelets, and despite the fact that their performance is inferior to that of quantum dots, such materials capped with octylamine were sufficiently stable that it was possible to fabricate them in an air atmosphere[15].

In regard to current efficiency, it was shown in 2015 that 42.9 cd A^{-1} could be achieved for green-light emitting LEDs, based on a hybrid organic–inorganic perovskite film[18], and while such devices still outshine LED devices made from inorganic ($CsPbBr_3$) perovskite nanocrystals, marked improvements have been obtained for the latter type of materials. Thus, the first green emitting $CsPbBr_3$ nanocrystal LED was reported in 2015, with a current efficiency of 0.43 cd A^{-1} (see ref. 19), but this had risen to 13.3 cd A^{-1} for such devices[20], in the space of only a year. Impressive though this is, in terms of the creation of practical devices based on perovskite nanocrystals, as yet, there remain numerous questions regarding the detailed mechanisms of how the materials degrade, how their colour properties might be stabilised, which methods might be devised by which to fabricate efficient and robust blue and red LEDs, and the most effective means to optimise the architecture for perovskite-based LED devices, more generally. Meanwhile, novel perovskite formulations and architectures continue to evolve,

and thus, it has been shown[21] that, by a combination of an appropriate choice of composition, phase engineering, and passivation of the perovskite film surface (an effective means to reduce defects in perovskite solar cells) using trioctylphosphine oxide, it is possible to create a quasi-two-dimensional hybrid organic–inorganic $PEA_2(FAPbBr_3)_{n-1}PbBr_4$ [where PEA and FA are phenylethylammonium ($C_6H_5C_2H_4NH_3^+$) and formamidinium ($HC(NH_2)_2^+$), respectively] perovskite with a current efficiency of 62.4 cdA^{-1} and an external quantum efficiency of 14.36% (see ref. 22). The stability and overall operational lifetime of perovskite nanocrystal LEDs is a major issue, although in comparison with the amount of similar work on perovskite solar cells, far more research is required to understand the degradative mechanisms which operate as a result of the operation of LEDs, their exposure to air, and while they are being stored (the so called 'shelf-life'). Thus, it is salient that when mixed halide perovskites are used for colour tuning, it has been reported that the emission colour becomes unstable after only a few seconds of operation[23].

5. Perovskites for use in phosphors and light-converting layers

Phosphor-based, solid-state, white LEDs provide a much higher efficiency alternative to both incandescent and fluorescent sources of illumination, but there are presently very few examples reported in the literature of white light emitting perovskite layers, which are based on $CsPbX_3$ (X = Br, I or Cl) either in the form of inorganic nanocrystals[23,24], hybrid perovskite nanocrystals, or hybrid methyl and octylammonium crystals with meso- to nano-dimensions[25]. However, it is the ability to tune the emission wavelength of the perovskite, either according to the halide composition, or by varying the size/shape of the nanocrystal, that has been exploited in all cases so far. Thus, it has been demonstrated that perovskite LEDs can be fabricated with colour-rendering indices in excess of 80, and colour temperatures in the range 5000–6000 K, which are comparable with other white light emitting LEDs currently on the market. As a consequence of their relatively fast (< 10 ns) PL lifetime, $CsPbBr_3$ nanocrystals have been employed as phosphors in a visible light communication system (VSL)[26], which aims to avoid some of the restrictions in data handing and wireless communication that are a feature of conventional IR-based networks. The proposed system uses a combination of perovskite nanocrystals and conventional phosphors, to achieve rapid emission rates and a large bandwidth of 491.4 MHz, which is significantly greater than for conventional nitride-based phosphors (~ 12.4 MHz), organic materials (40−200 MHz) or doped yttrium aluminium garnet (YAG)-based phosphors (3−12 MHz) (ref. 26).

6. Perovskite-based lasers

Various recent studies have demonstrated that organic–inorganic metal halide perovskites are promising optical-gain materials for use in lasers. Thus, a study was made of $CH_3NH_3PbI_3$ films, which showed that the amplified spontaneous emission (ASE) threshold carrier density might be as low as ~ 1.7×10^{18} cm^{-3}, which implies that the gain should be sufficient to produce an efficient working laser[27]. Low lasing

thresholds of < 200 μJ cm^{-2} per pulse, with a very narrow linewidth of less than 0.5 nm, were reported for the $CH_3NH_3PbI_3$ perovskite[27], while a laser response was obtained from $CH_3NH_3PbX_3$ nanowires at a threshold of only 220 nJ cm^{-2}, which is remarkably low and corresponds to a carrier density of perhaps only 1.5 × 10^{16} cm^{-3}. Such perovskite nanowires also contain very few carrier trapping sites, and it is estimated that the quantum yield for lasing is practically 100% (see ref. 15). It has been proposed that the good performance of perovskite nanowires and nanoplatelets, as self-lasing materials, is due to their high degree of crystallinity, in addition to a high optical gain[27]. Zhang *et al.* reported[28] a near infra-red solid state nanolaser device, based on nanoplatelets of $CH_3NH_3PbI_{3-x}X_x$ (X = I, Br, Cl), in the form of microdisks that can operate in a whispering gallery mode (WGM), which demonstrated both a large exciton binding energy and an appreciable diffusion length, along with satisfactory quantum yields, thus rendering the material as a good candidate for a WGM laser. In order to address the issue of water sensitivity in such devices, a water-resistant polymer thin-film, with good flexibility and transmission performances, was emplaced onto polygonal microdisks, to create a very effective built-in WGM microresonator for laser production[28].

A distributed feedback cavity (DFB) structure was pionered[29] by Kogelnik *et al.*, as far back as 1971, and was recently attained practically[30] by Saliba *et al*., which is significant in that such cavities made from perovskites offer to provide mirror free, widely tunable, and single mode lasers, relatively cheaply and at scale. The versatility of the DFB structure offers the possibility of being optimised to achieve lower thresholds or varying output energies. Through the exploitation of different known organic–inorganic perovskites, and by tailoring the cavity to the gain maximum of the unpatterned film, a broad tunability of the laser might prove possible. It has been proposed that improved performances of lasers might be achieved by means of alternative cavity configurations, and an improved stability of the organic–inorganic hybrid perovskite materials, with potential future applications for sensor, display, and lab-on-chip applications. Research has also been undertaken with the aim to improve the quality factor in lasers based on perovskite microcrystals[31], perovskite microrods[32] and perovskite quantum dot LEDs[33].

7. Perovskite dynamics

In the crystal structure of $CH_3NH_3PbX_3$, each methylammonium cation ($CH_3NH_3^+$) is surrounded by PbX_6 octahedra and can rotate within the cage in which it is held (Figure 1); however, the X ions are not fixed in position and can migrate through the crystal with an activation energy of 0.6 eV, a process that is vacancy assisted[34]. The methylammonium cations are able to rotate within their cages: thus, at room temperature, the CN axis of the methylammonium cation is aligned towards the face directions of the unit cells, but this orientation changes on a random basis to another of the six face directions on a timescale[35] of 3 ps. The overall issue of molecular motion, and ion/electron/hole transport in perovskites, is complex, as has been addressed in detail in a review[36] with the apposite title 'What is moving in hybrid halide perovskite solar cells?' A particular feature of hybrid halide perovskites is that,

unlike more conventional semiconductors, they are physically 'soft', which permits molecular motion of various kinds to occur, that are driven by thermal activation. In particular, methylammonium lead iodide ($CH_3NH_3PbI_3$) and formamidinium lead iodide ($[CH(NH_2)_2]PbI_3$) both display molecular rotation-libration in the cuboctahedral cavity, drift and diffusion of large electron and hole polarons, and the transport of charged defects. It is the combination of these dynamic features which confers various properties, such as a permittivity that is frequency-dependent, low rates for electron–hole recombination events, and current–voltage hysteresis, all of which are not typically found with photovoltaic materials[36]. The different motional processes are characterised by specific timescales, and thus the motion of electrons and holes occurs within femtoseconds, the libration of molecules requires less than a picosecond, while the rates of molecular rotations are cation-dependent but are of the order several picoseconds (Table 1).

There is both an experimental and theoretical basis from which to infer that electron and ion transport in these materials may occur concurrently, leading to the interesting conclusion that they are mixed-mode conductors, and thus bear some relation to the kind of fast-ion conducting metal oxide perovskites that are being evaluated for potential use in fuel cells and batteries. It is found that there are large differences between the average crystal structures, and those which exist on the local scale. Furthermore, the one-dimensional drift-diffusion models that are commonly employed, do not account for the far more complex charge transport processes that occur in perovskites. At > 1 μm (see ref. 33), the minority-carrier diffusion lengths are surprisingly large, especially for a material that is a direct band gap semiconductor, and which also must contain numerous structural defects as a result of its having been fabricated by solution processing. However, it is because this diffusion length is greater than the thickness of the film required for full solar spectrum absorption, that methylammonium lead iodide and formamidinium lead iodide are well suited for photovoltaic applications. It has been concluded that the principal mechanism for carrier-scattering involves acoustic phonons[37]: on the basis of measurements of the temperature dependences of transport processes, and of the time constants for transient recombination, it was concluded that, under conditions of normal sunlight, a monoexponential, monomolecular process of electron–hole recombination occurs, while at greater light intensities, the recombination is biexponential, and therefore bimolecular[38]. Most importantly, the data provide evidence for an internal mechanism that suppresses direct electron–hole interactions[37].

8. Large area perovskite solar cells

Efforts are currently underway to manufacture perovskite solar cells on the large scale, in order to achieve practical electricity production from such devices in the future[39]. The developments in improved composition and morphology of perovskite thin films, which have been made largely due to advances in solution-based chemistry and in the overall fabrication process, which have driven a remarkable improvement in the efficiency of small-area devices, have now been employed for large-area versions, and resulted in a parallel trend in their improvement. It is expected that a

Table 1 *Summary of dynamic processes and estimates of their associated time constants, in* $CH_3NH_3PbI_3$

Process	Microscopic origin	Time scale	Frequency	Diffusion coefficient
Lattice vibrations	Vibrational entropy	10 fs to 1 ps	1−100 THz	–
Molecular libration	Vibrational entropy	0.5 ps	2 THz	–
Molecular rotation	Rotational entropy	3 ps	0.3 THz	–
Electron transport	Drift and diffusion	~1fs	~1000 THz	10^{-6} cm^2 s^{-1}
Hole transport	Drift and diffusion	~1fs	~1000 THz	10^{-6} cm^2 s^{-1}
Ion transport	Drift and diffusion	~1ps	~1 THz	10^{-12} cm^2 s^{-1}

loss in efficiency will occur when a solar cell is scaled up, primarily due to a number of combining factors, including a higher series resistance, a lower shunt resistance, that the coating over a larger area will be less uniform, and that the greater area accounted for by bus bars and interconnections equates to a significant fraction of the total cell area that is photovoltaically inactive ('dead regions')[39]. In general, the efficiencies of various different types of solar cells appear to decrease inversely with scale, and amount to around 0.8% for each order of magnitude increase in the area of the device. However, for perovskite solar cells, the loss in efficiency that occurs as the area increases is worse than this, but it is thought that this is simply due to a relative paucity of research into the scaling-up of the devices, as compared with other types of solar cell. Among the various different approaches to enable scalable solution-deposition for perovskites are: slot-die coating, blade coating, meniscus coating, spray coating, electrodeposition, inkjet printing, and screen printing, although this list is far from being exhaustive[39]. We may note, however, a recent report in which a soft polymer sheet was used to cover the coating substrate and trap the precursor ink between the layers, before the coating was applied. Thus, the resulting meniscus liquid edge was caused to move when the polymer sheet was slowly peeled off, resulting in perovskite thin films that were uniform, and with an area of up to 51 cm^2 (see ref. 40). Success has also been achieved recently, using solvent systems with ultrafast evaporation rates for the production of large scale perovskite solar cells. Thus, a soft cover was used to spread $MAPbI_3$–CH_3NH_2 which, under high pressure, is a liquid, and to produce a uniform film of $MAPbI_3$ over a substrate area of 8 cm × 8 cm; the method was used to create[41] a perovskite solar cell module with certified aperture power conversion efficiency (PCE) of 12.1% (~ 90% geometric fill factor [GFF], *i.e.* the ratio of the active area to the total substrate area of the module; a higher GFF means a smaller dead area and, therefore, less power reduction as a result of integration of the module)[42]. Another group[43] has reported the fabrication of perovskite modules by means of spray coating a TiO_2 electron transport layer and then blade coating both a perovskite absorber layer and a spiro-OMeTAD-based hole transport layer [spiro-OMeTAD = N^2,N^2,$N^{2'}$,$N^{2'}$,N^7,N^7,$N^{7'}$,$N^{7'}$-octakis(4-methoxyphenyl)-9,9′-spirobi[9H-fluorene]-2,2′,7,7′-tetramine]. An improved performance was found for those perovskite modules with a TiO_2 layer of thickness

10 nm, which was associated primarily with an enhanced fill factor. In addition, a four-cell $MA_{0.7}FA_{0.3}PbI_3$ perovskite module was demonstrated, which yielded a stabilised PCE of 15.6%, as measured from an aperture area of ~10.36 cm^2, and which accorded with an active-area PCE of 17.9% (according to a GFF of ~ 87.3%).

9. Perovskite catalysis for pollutant degradation

Photocatalysis may be defined as the 'acceleration of the rate of a photochemical reaction by the presence of a catalyst', and the absorption of light by an appropriate semiconductor (SC) particle may result in the generation of positive holes and electrons. The crucial parameter for determining the potential viability of a photocatalyst is the energy spacing ('band gap') between the conduction band (cb) and the valence band (vb), and when a photon carrying sufficient energy to match this gap is absorbed, a positive 'hole' (electron vacancy) is created in the vb while an electron is transferred to the cb (Eqn 1)[44].The holes can oxidise water to form $HO^{\bullet}$ radicals (Eqn 2), while the electrons may be scavenged by O_2 molecules to form superoxide radical anions ($O_2^{-\bullet}$). $HO^{\bullet}$ radicals are fiercely oxidising and can decompose a wide range of organic molecules (*e.g.* Figure 4), ideally converting them ultimately to $CO_2 + H_2O$ (full mineralisation).

Considerable efforts have been made to optimise photocatalytic systems for use in cleaning water of organic pollutants. The essential requirement is that the solution should be air-saturated, and contain suspended particles of a semiconductor to serve as the photocatalyst, the most commonly employed such material being titanium dioxide[44]. Since the 'band-gap' (excitation energy) for TiO_2 is 3.2 eV, which corresponds to a wavelength of *ca* 400 nm, and is at the border of the UV/visible spectrum, efforts are currently being made to find catalysts with a smaller band-gap, such that (far cheaper) visible light can be used for various purposes, including pollutant degradation and energy generation applications[45].

$$SC + h\nu \rightarrow e^-_{CB}(SC) + h^+_{VB}(SC) \qquad \text{Eqn (1)}$$

$$h^+_{VB}(SC) + H_2O\ (-\ e^-) \rightarrow [H_2O^{+\bullet}] \rightarrow HO^{\bullet} + H^+ \qquad \text{Eqn (2)}$$

A novel organic–inorganic heterojunction photocatalyst has been explored[46], which employs $CaTiO_3$ (CT) nanoflakes deposited onto the surface of g-C_3N_4 nanosheets. The greatest photocatalytic activity was found for a 1:1 ratio of g-C_3N_4/$CaTiO_3$, which was effective in the degradation of bisphenol-A, which is a colourless, non-photosensitising pollutant. The efficiency of this photocatalyst can be attributed to several factors, including suitably positioned absorption bands, close contact at the interface between the organic–inorganic components, light absorption in the visible and UV ranges (which in combination inhibit the recombination of photogenerated charges, by assisting their transfer across the heterojunction), along with the large surface area that is provided by the two-dimensional arrangement of g-C_3N_4 nanosheets and CT nanoflakes, which enhances the overall catalytic activity by furnishing more reaction sites. It is of interest that, rather than $HO^{\bullet}$ being the dominant active agents involved in the

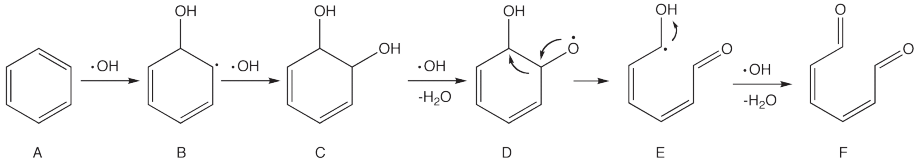

Figure 4 *Mechanism for the degradation of benzene by hydroxyl radicals. Credit: Daniel.Rico, https://upload.wikimedia.org/wikipedia/commons/b/b9/Mechanism_of_OH_with_benzene.png.*

pollutant photodegradation processes, it was demonstrated that superoxide radical anions ($O_2^{-\bullet}$) were the major species involved[46]. The visible-light driven removal of styrene, as a pollutant from air, has been reported, which was accomplished using ABO_3-type perovskite (A = La, Ce, Sm; B = Cr, Mn, Fe, Co, Ni) catalysts[47]. Other workers have reported[48] the degradation and mineralisation of phenol, as present in water, *via* heterogeneous monopersulfate activation on nanostructured cobalt based-perovskite catalysts $ACoO_3$ (A = La, Ba, Sr and Ce)**,** with an activity order of $SrCoO_3$ > $LaCoO_3$ > $BaCoO_3$ > $CeCoO_3$. $LaCoO_3$ and $SrCoO_3$ catalysts were found to be the most effective, regarding both reaction rate and stability for the degradation and mineralisation of phenol, and through the use of radical scavengers, it was established that reactive oxygen species, mainly $SO_4^{\bullet-}$ and $HO^{\bullet}$, were involved in the process. Four organic degradation products were detected, three of which were identified to be catechol, hydroquinone and benzoquinone; it was proposed that attack on these species by $SO_4^{\bullet-}$ radicals produced smaller molecules such as, acetic acid, formic acid, and oxalic acid, which were identified by ion-exclusion chromatography[48].

A study was made[49] of the orientation-dependent structural and photocatalytic properties of $LaCoO_3$ epitaxial nano-thin films, which had been grown on (100), (110) and (111) oriented $LaAlO_3$ substrates by the method of polymer-assisted deposition. The three different film orientations were found to behave differently toward the degradation of methyl orange, the most effective being the (100) oriented LCO film, which resulted in a 99.06% removal after irradiation for 7 h. This was reduced to 95.71% for the (110) orientation, while an intermediate degree of degradation was achieved using the (111) orientated film[49]. It was reported[50] that by doping the perovskite, $BaSnO_3$, with Fe^{3+} cations, improvements could be made in its photocatalytic properties. On the basis of X-ray diffraction (XRD) and Raman measurements, it appeared that the Fe^{3+} cations had entered the lattice of the perovskite, causing a reduction in the band gap energy. The photodegradation of an azo-dye was used to study the effectiveness of the catalyst, and at pH = 3, it appeared that the indirect mechanism (involving the production of reactive oxygen species, such as hydroxyl radicals) was dominant, and it was thought that the presence of the Fe^{3+} cations improved the efficiency of the catalyst due to the creation of intermediate levels within the band gap, which may serve as electron traps, and thus impede electron-hole recombinations[50]. The effective degradation of organic pollutants using a system containing H_2O_2 and a Cu-doped $LaAlO_3$ perovskite catalyst has been demonstrated[51], which proceeds *via* heterogeneous Fenton-type reactions, leading to the formation of hydroxyl radicals. It was

concluded that HO• radicals were formed by the reduction of H_2O_2 on the electron-rich Cu centre, but that oxygen vacancies that are present can cause the dissociation of H_2O_2/H_2O to form additional HO• radicals, and the combination of these routes confers a high activity to the $LaAl_{0.95}Cu_{0.05}O_3$ catalyst[51].

10. Stability of perovskites under actual working conditions

Although hybrid perovskites such as $CH_3NH_3PbI_3$ offer a tremendous potential for solar energy conversion, the rapid degradation of these materials which occurs when they are exposed to normal atmospheric conditions (with or without sunlight), poses a current limitation to their use in practical applications. Both chemical and thermodynamic factors may be responsible for the degradation processes, but hope is offered by a number of recent studies that suggest it should prove possible to realise a greater longevity of these materials, for example by amending the gaseous environment or by tuning the nature of the surface/interface. On the basis of a critical analysis[52] of various relevant data, it has been concluded that, under ambient conditions, the degradative mechanisms are driven by highly localised defects, present on surfaces and interfaces, and that an enhancement of the process occurs above the tetragonal-cubic transition temperature (~ 54 °C). It is proposed that N_2 gas can serve a protective role, and strategies are suggested for the engineering of hybrid photovoltaics, which might be achieved on an industrial scale[52]. Another group has made a study[53] of the long-term stability of ITO/SnO_2/$Cs_{0.05}((CH_3NH_3)_{0.15}(CH(NH_2)_2)_{0.85})_{0.95}PbI_{2.55}Br_{0.45}$/spiro-OMeTAD/Au cells, as present in the open-air environment, along with their degradation dynamics, using simulated sunlight (indoors) and their recovery in the dark. It was found that both light-driven processes and those occurring in the dark (as in daytime and night-time) are responsible for the degradation, but that the dynamics of the process change as the cell ages. Thus, in the early stages of degradation, it is possible to obtain a recovery of full conversion efficiency, while as the process advances, the degradation is irreversible under actual working conditions. Due to the interplay of reversible and irreversible degradation processes, changes in the cell's diurnal light conversion efficiency occur over the course of the operational lifespan of the cell[53]. In order to circumvent the influence of water on the degradation of perovskite solar cells, an unencapsulated device, with a tailored interface, has been presented which was able to still deliver 94% of its starting PCE, even after 1,000 hours of operation, under ambient conditions (relative humidity 10–20%)[54]. As an alternative approach[55] to making air-stable perovskite solar cells, a group in South Korea has devised a co-precipitation method in order to create a thin film that employs nanoporous nickel oxide as the hole transporting layer (HTL), and a mixture of methylammmonum lead iodide and formamidinium lead bromide as the perovskite layer, along with a layer of zinc oxide nanoparticles as the electron transporting layer (ETL), which protects the perovskite layer from the air. A power conversion efficiency of 19.1% was obtained[55].

11. Avoiding toxic materials

The presence of lead in perovskites such as methylammmonum lead iodide and formamidinium lead bromide raises issues about the toxicity of these materials for practical applications, and hence there is an active search being undertaken by many groups for lead-free alternatives. Among the recent developments may be mentioned the use of lead-free perovskites, based on divalent chalcogenides and monovalent halides, in which 3^+ and 4^+ charged cations are substituted for 2^+ metal cations, particularly Pb^{2+}. Thus, solar cells have been described which use the methylammonium antimony sulfur diiodide ($MASbSI_2$) perovskite as a light harvesting material, and which provided a PCE of 3.08%, under standard illumination conditions (100 mW cm^{-2}) (see ref. 56). Though far lesser known than perovskites, kesterites[57] have also been explored for their use in the fabrication of solar cells. Thus we see that just over 1,000 papers were published during the past five years on kesterites (with a record PCE of 12.6%), while there were almost 6,000 papers published on perovskites (with a record PCE of 22.1%) (see ref. 57). Kesterites are very stable, and derived from earth-abundant elements such as copper, zinc, tin, and sulfur (Cu_2ZnSnS_4; frequently given the abbreviation CZTS). Some large-scale projects have been inaugurated to develop kesterite-based solar cells, the major one being 'Starcell', which involves a consortium of universities and private organisations in Europe, with the aim to attain a PCE of 18% by 2020; however, a rival project based in Australia has the more lofty goal, of achieving a PCE of 20% by 2022. The materials are fraught with difficulties, however, in particular due to the formation of structural defects that hamper their photovoltaic performance, and so there are many challenges to be met if kesterites are to become major players in the global PV arena[57].

Published online: ## #### 201#

12. References

1. Rhodes, C.J. (2014) *Sci. Prog.*, **97**, 279–287.
2. Rhodes, C.J. (2016) *Sci. Prog.*, **99**, 335–345.
3. Rhodes, C.J. (2018) *Sci. Prog.*, **101**, 192–204.
4. Zhou, D., Zhou, T., Tian, Y., *et al*. (2018) *J. Nanomater*., **2018**, Article ID 8148072, https://doi.org/10.1155/2018/8148072.
5. Cintelliq (2018) *The OSADIRECT Newsletter*. 17 July. http://www.osadirect.com/news/article/2102/perovskite-photovoltaic-a-review-of-the-patent-landscape-2018-q1-now-includes-patents-to-dec-2017/ [accessed 17 July 2018].
6. Wells, H.L (1893) *Z. Anorg. Allg. Chem*., **3**, 195–210.
7. Kojima, A., Teshima, K., Shirai, Y. and Miyasakaet, T. (2009) *J. Am. Chem. Soc*., **131**, 6050–6051.
8. Prato, M. and Di Stasio, F. (2017) *LED Professional*. 18 May. https://www.led-professional.com/resources-1/articles/lead-halide-perovskite-nanocrystals-a-new-promise-for-light-emitting-devices [accessed 17 July 2018].
9. National Renewable Energy Laboratory (2018) NREL efficiency chart. https://www.nrel.gov/pv/assets/images/efficiency-chart.png [accessed 17 July 2018].
10. Quiroz, R., Omar, C., Yilei, S., *et al.* (2018) *J. Mater. Chem. A*., **6**, 3583–3592.

11. Sahli, F., Werner, J. and Kamino, B.A. (2018) *Nature Mater*., https://doi.org/10.1038/s41563-018-0115-4.
12. Solliance (2018) Solliance sets 14.5% cell performance record on large perovskite modules https://solliance.eu/solliance-sets-14-5-cell-performance-record-on-large-perovskite-modules/ [accessed 17 July 2018].
13. Shockley, W. and Queisser, H.J. (1961) *J. Appl. Phys*., **32**, 510–519.
14. Tan, Z.-K., Moghaddam, R.S., Lai, M.L., *et al*. (2014) *Nat. Nanotechnol.*, **9**, 687–692.
15. Ha, S.-T., Su, R., Xing, J., *et al*. (2017) *Chem. Sci*., **8**, 2522–2536.
16. Rhodes, C.J. (2010) *Sci. Prog*., **93**, 37–112.
17. Protesescu, L., Yakunin, S., Bodnarchuk, M.I., *et al.* (2015) *Nano Lett*., **15**, 3692–3696.
18. Cho, H., Jeong, S.H., Park, M.H., *et al*., (2015) *Science*, **350**, 1222–1225.
19. Song, J., Li, J., Li, X., *et al*. (2015) *Adv. Mater*., **27**, 7162–7167.
20. Li, J., Xu, L., Wang, T., *et al*., (2017) *Adv. Mater*., **29**, 1603885.
21. Yang, X., Zhang, X., Deng, J., *et al*. (2018) *Nat. Comm*., **9**, 570.
22. Li, G., Wisnivesky, F., Rivarola, R., *et al*. (2016) *Adv. Mater*., **28**, 3528–3534.
23. Song, Y.H., Yu, J.S., Kang, B.K., *et al*. (2016) *Nanoscale*, **8**, 19523–19526.
24. Palazon, F., Di Stasio, F. and Akkerman, Q.A. (2016) *Chem. Mater*., **28**, 2902–2906.
25. Pathak, S., Sakai, N., Wisnivesky, F., *et al*. (2015) *Chem. Mater*., **27**, 8066–8075.
26. Dursun, I., Shen, C., Parida, M.R., *et al*. (2016) *ACS Photonics*, **3**, 1150–1156.
27. Sun, J., Wu, J., Tong, X., *et al*. (2018) *Adv. Sci*., **5**, 1700780.
28. Zhang, Q., Ha, S.T., Liu X., *et al*. (2014) *Nano Lett*., **14**, 5995–6001.
29. Kogelnik, H. and Shank, C.V. (1971) *Appl. Phys. Lett.*, **18**, 152–154.
30. Saliba, M., Wood, S.M., Patel J.B., *et al.* (2016) *Adv. Mater*., **28**, 923–929.
31. Zhang, Z-Y., Wang, H.-Y., Zhang, Y.-X., *et al*. (2017) *Phys. Chem. Chem. Phys*., **19**, 2217–2224.
32. Zhang, C., Wang, K., Yi, N., *et al*. (2016) *Adv. Opt. Mater.*, **4**, 2057.
33. Deng, W., Xu, X., Zhang, X., *et al*. (2016) *Adv. Funct. Mater*., **26**, 4797–4802.
34. Eames, C., Frost, J.M., Barnes, P.R.F., *et al*. (2015) *Nat. Comm*., **6**, 7497.
35. Bakulin, A.A., Selig, O., Bakker, H.J., *et al*. (2015) *J. Phys. Chem. Lett.*, **6**, 3663–3669.
36. Frost, J.M. and Walsh, A. (2016) *Acc. Chem. Res.*, **49**, 528–535.
37. Karakus, M., Jensen, S.A. and D'Angelo, F. (2015) *J. Phys. Chem. Lett.*, **6**, 4991−4996.
38. Stranks, S.D. and Snaith, H.J. (2015) *Nat. Nanotechnol*., **10**, 391−402.
39. Li, Z., Klein, T.R., Kim, D.H., *et al*. (2018) *Nat. Rev. Mater*., **3**, 18017.
40. Ye, F., Chen, H., Xie, F., *et al*. (2016) *Energy Environ. Sci*., **9**, 2295–2301.
41. Chen, H., Ye., F., Tang, W., *et al*. (2017) *Nature*, **550**, 92–95.
42. Uličná, S., Dou, B., Kim, D.H., *et al*. (2018) *ACS Appl. Energy Mater*., **1**, 1853–1857.
43. Yang, M., Kim, D.H., Klein, T.R., *et al*. (2018) *ACS Energy Lett*., **3**, 322–328.
44. Rhodes, C.J. (2011) *Sci. Prog*., **94**, 339–413.
45. Rhodes, C.J. (2013) *Sci. Prog*., **96**, 309–316.
46. Kumar, A., Schuerings, C., Kumar, S., *et al*. (2018) *Beilstein J. Nanotechnol*., **9**, 671–685.
47. Chen, J., He, Z., Li, G., *et al.* (2017) *Appl. Catal. B Environ.*, **209**, 146–154.
48. Hammouda, S.B., Zhao, F., Safaei, Z., *et al*. (2017) *Appl. Catal. B Environ.*, **215**, 60–73.
49. Zhang, Y.-P., Liu, H.-F., Hu, H.-L., *et al*. (2018) *R. Soc. Open Sci*., **5**, 171376.
50. Moira, K.F., Chantelle, L., Rosendo, D., *et al.* (2017) *Mater. Res*., **20** (Suppl. 2), 317–324.
51. Wang, H., Zhang, L. and Hu, C. (2018) *Chem. Eng. J*., **332**, 572–581.
52. Deretzis, I., Smecca, E., Mannino, G., *et al.* (2018) *J. Phys. Chem. Lett*., **9**, 3000−3007.
53. Khenkin, M.V., Anoop, K.M., Visoly-Fisher, I., *et al.* (2018) *ACS Appl. Energy Mater.*, **1**, 799–806.
54. Christians, J., Schulz, P., Tinkham, J.S., *et al*. (2018) *Nature Energy*, **3**, 68–74.
55. Mali, S.S., Kim, H., Kim, H.H., *et al*. (2018) *Mater. Today*, **21**, 483–500.
56. Nie, R., Mehta, A., Park, B.-W., *et al*. (2018) *J. Am. Chem. Soc*., **140**, 872–875.
57. Peplow, M. (2018) *Chem. Eng. News*, **96**, 15–18.